Practical guide to understanding goodness-of-fit metrics used in chemical state modeling of x-ray photoelectron spectroscopy data by synthetic line shapes using nylon as an example

N. Fairley, P. Bargiela, A. Roberts, V. Fernandez, J. Baltrusaitis

Practical Guide to Understanding Goodness-of-Fit Metrics used in Chemical State Modelling of X-ray Photoelectron Spectroscopy (XPS) Data by Synthetic Line Shapes Using Nylon as an Example

Neal Fairley,[1] Pascal Bargiela,[2] Adam Roberts[3], Vincent Fernandez,[4] and Jonas Baltrusaitis[5]

[1]Casa Software Ltd, Bay House, 5 Grosvenor Terrace, Teignmouth, Devon TQ14 8NE, UK
[2]The Institute for Research on Catalysis and the Environment of Lyon (*IRCELYON)*, 2 Avenue Albert Einstein, 69626 Villeurbanne, France
[3]Kratos Analytical Ltd, Manchester, UK
[4]Université de Nantes, CNRS, Institut des Matériaux Jean Rouxel, IMN, F-44000 Nantes, France
[5]Department of Chemical and Biomolecular Engineering, Lehigh University, 111 Research Drive, Bethlehem, PA 18015, USA

Abstract

Chemical state analysis of the sample surface using fitting bell-shaped curves to polymer data is reviewed and placed into the context of the X-ray Photoelectron Spectroscopy technique. A specific example of Nylon is selected by which aspects of data analysis are introduced and discussed. Different strategies for modelling chemistry in Nylon spectra are presented and in so doing, a case is made to include in published science the design logic and implementation in terms of line shapes and optimization parameter constraints between components in a peak model. Imperfections in line shape relative to the true shape for photoemission lines, when compensated for using constraints to optimization parameters, are shown to provide chemical state information about a sample and that, for peak models constructed with these limitations, metrics for goodness-of-fit different from that expected for pulse counted data can be justified.

Introduction

An assumption that uncertainties in X-ray Photoelectron Spectroscopy (XPS) are described by Poisson distributed noise is equivalent to an assumption that an XPS measurement has been performed under strict and ideal conditions. In practice, XPS is performed under less-than-ideal conditions and therefore goodness-of-fit metrics, that support the use of a particular peak model in understanding the chemistry of a sample, often returning a suboptimal fit to data.[1,2] Nonetheless, a suboptimal fit for a peak model to data may still provide a valid interpretation of chemistry. Therefore, the problem for an analyst is to decide whether or not a suboptimal fit implies a valid peak model has been used to fit data. In this manuscript, the relationship is examined between X-ray Photoelectron Spectroscopy (XPS) data, the assumption that XPS is performed under a pulse counting regime and the conditions under which XPS data conforms to a statistical model for pulse counted data.[3,4]

XPS data available in the Beamson and Briggs, XPS of Polymer Database, include many examples of C 1s photoemission spectra, where electrons in an atom, on scattering by photons of precise energy, create data envelopes with shapes open to analysis by fitting bell-shaped curves to data. The use of bell-shaped curves in the analysis of spectra is

appropriate for materials where there is a one-to-one correspondence between the energy of each bell-shaped curve and the chemistry of the atom from which the photoelectrons are emitted. The caveat to this paradigm for chemical state analysis is photoemission peaks in spectra do not always appear in isolation from photoemission signals corresponding to different chemical states of atoms. Many chemical states involving carbon, oxygen and nitrogen (in particular) contribute to photoemission signals from carbon that overlap in energy. When presented with complex spectral shapes, the solution, especially for polymers, is to construct a peak model using sets of bell-shaped curves and through the use of nonlinear optimization, separate signals into units that can be assigned to the chemical state. While spectra in the Beamson and Briggs database[5] range from simple spectra with isolated photoelectron peaks to complex spectra for which ensembles of peaks from numerous chemical states are required, a discussion aimed at general principles used in fitting curves to data is best performed using a specific case study. Therefore, an example of such a polymer for which spectra exhibit enough complexity to warrant the use of modelling by bell-shaped curves and yet are still simple enough to be open to chemical interpretation with ease is Nylon and C 1s spectra from Nylon. The following, therefore, makes use of experiments performed on Nylon samples to explain aspects of XPS measurement and how analysis of XPS data is performed using peak models and nonlinear optimization.

In particular, the objective of this manuscript is to present a peak model that describes adequately the chemistry of Nylon while falling short of achieving goodness-of-fit metrics expected for pulse counted data (see video 1 (V1) in the supplementary material for fitting statistics for pulse counted data. The construction of the peak model (see V2 in the supplementary material for peak model creation and parameters constraints) and how such a peak model is justified is central to the thesis of this manuscript. Therefore, the general ideas that are used during the analysis of spectral data using fitting bell-shaped curves to XPS data[6] are presented. In doing so, the readers may make a judgement to the validity of the assertion that a peak model when fitted to data with goodness-of-fit metrics less-than-optimal, is capable of returning valuable information about a sample. The detail provided is intended to emphasize that the conclusions drawn from a peak model are only valid if the assumptions used in constructing the peak model are valid. Throughout this manuscript, data are presented using the apparent binding energy scale determined by the instrument and charge-compensation conditions used to acquire spectra. Presenting data in terms of apparent binding energy represents information about how data were acquired, which is more important when assessing shapes in data than if all data are presented using a unified binding energy scheme created by calibration post-acquisition. While understanding sample chemistry may be enhanced by calibration to a unified binding energy scale[7] for all data, the focus for this manuscript is constructing peak models and understanding fitting-statistics. Avoiding pre-processing of data in any form is preferable for the themes germane of this paper.

Methods

Fitting Statistics for Pulse Counted Data

Most modern instruments measure signals using event counting.[8] An electron of given energy arrives at the detection system and, if detected, is recorded by adding one count to a given data bin within a spectrum. An electron arriving at the detector must enter an electron-multiplier (channel plates) that creates a cascade of electrons which triggers a response in electronic circuits. If the pulse of electrons from the electron-multiplier is above a given threshold, the electron is detected. Detectors may add spurious counts due to any physical event (not due to the arrival of an electron at the detector) that triggers a cascade of electrons within the electron-multiplier. These spurious counts are referred to as detector background noise. There are also situations where a detector fails to record electrons. If the number of electrons arriving at the detector means that the time interval between successive electrons is smaller than the time required by the electron-multiplier and electronics to recover from the first electron, then the second electron is not recorded. The time interval required for a detector to reset in preparation for recording an electron is referred to as detector dead-time. However, provided an instrument is performing correctly and the operating mode, used to transfer electrons from the sample to the detector, limits the number of electrons available for detection, then spectra acquired under these conditions are described as *pulse counted* electrons. Uncertainty in the number of electrons recorded by pulse-counting electrons is described statistically as being modelled by a Poisson distribution.[9] The importance of recognizing the validity of this assertion is that statisticians can justify the statement that given the number of counts per data-bin, the uncertainty in the number of counts per data-bin is proportional to the square root of the counts in that data-bin. Understanding the uncertainty in the counts per data bin then allows a target value for a figure-of-merit, in the form of Equation (1) used during optimization, to indicate the fit of a curve to data is optimal in a mathematical sense

$$Residual\ StDev = \sqrt{\frac{1}{n}\sum_{i=1}^{n}\left(\frac{d_i - e_i}{\sqrt{d_i}}\right)^2} \qquad (1).$$

If a curve fits data such that the residual standard deviation (STD) is unity, then for pulse counted data the solution is optimal. The reason the target of unity (see V3 in supplementary material for the reason residual STD is expected to be unity for pulsed counted data) is appropriate for pulse counted data is the operand in the summation in Equation (1) measures the distance between the curve e_i and the data d_i divided by the statistically predicted distance between these two quantities. For pulse counted data, the difference between the curve e_i and the signal in a data bin d_i is predicted to be $\sqrt{d_i}$. If this expectation for the difference between the curve and data is met, then the operand will, on average, yield unity. Hence, for an ideal fit of a curve to pulse counted data, Equation (1) is the sum of n terms each of which is equal to unity. Therefore, the residual standard deviation in Equation (1) will return a value of unity.

To make use of Equation (1) for XPS data it is necessary to demonstrate that XPS data meet the conditions required to model variations in data using Poisson statistics. The following three assertions must be true for XPS data to allow the use of Poisson statistics.

Given the characteristics of XPS spectra described above, it can be assumed there exist a count rate ν such that

1) The probability of a single counting event occurring in a small-time interval of length δt is approximately equal to $\nu\delta t$;
2) The probability of more than one counting event occurring in a small-time interval δt is negligible when compared to a single counting event occurring in the same time interval;
3) The numbers of counting events in non-overlapping time intervals are independent.

While the three conditions for the count rate ν appear abstract, each can be placed into the context of XPS. The first condition requires that the number of electrons counted is proportional to the count rate and duration-of-time counting is performed. This statement is fundamental to the statement that XPS is a quantifiable technique. Therefore, the first condition must be true for use of XPS to be valid. The second condition, placed in the context of XPS, asserts that electrons are recorded at a frequency that prevents detector saturation. Again, quantification by XPS depends on the use of an instrument for a given sample that prevents saturation of detectors. Dead-time correction is sometimes offered that estimates count for high count rates, but with reliable quantification by XPS, it is arguably better to use count rates for which dead-time correction is unnecessary. The final condition is a further requirement for the use of XPS, namely, we assume that measuring C 1s, for example, then O 1s at a different time result in counts for each that are independent of when these two measurements are performed. Thus, the basic use of XPS to measure sample chemistry and composition assumes the conditions for modelling variations in pulse counted data by a Poisson distribution are satisfied.

Given these assumptions, it can be shown that the number of counting events occurring in a period t has a Poisson distribution with parameter $\lambda = \nu t$. If the random variable $X(t)$ denotes the number of counting events in the time interval t then

$$P[X(t) = r] = \frac{e^{-\nu t}(\nu t)^r}{r!} \quad (2)$$

for $r = 0,1,2, \ldots$

Given that X is a Poisson distributed random variable, then the expected value and variance for $\lambda = \nu t$ are as follows

$$\mathcal{E}[X] = \lambda \quad (3)$$

and

$$var[X] = \lambda \quad (4).$$

Since for pulse counted XPS data λ corresponds to the counts per bin, the standard deviation in the counts per bin is

$$\sigma = \sqrt{var[X]} = \sqrt{\lambda} \quad (5).$$

Justification for the use of XPS as a quantifiable technique might therefore be seen in terms of fitting curves to data with fitting statistics compatible with Poisson statistics. Put another way, fitting curves to data without returning the behavior expected for pulse counted data might be seen as evidence an XPS instrument is not performing in an operational mode that would permit quantification. There are, however, reasons why fitting statistics can deviate from that expected for pulse-counted data without implying problems for the quantification of XPS data. Two examples are now presented which demonstrate Poisson statistics apply to these XPS data.

Two spectra shown in Figure 1 and Figure 2a are used to illustrate the Poisson-like behavior of XPS data. In both examples, an estimate for the signal is obtained by selecting energy intervals over which no photoemission resonance peaks are present. These energy intervals are used to fit linear polynomials independently to data in each energy interval. Variations in signal relative to these linear approximations are used to examine fitting statistics for XPS data.

An example of data where the noise is Poisson distributed is illustrated in Figure 1. Data shown in Figure 1 are acquired by summing all electron-induced events over a 2D delay line detector, one energy-data bin at a time. Count rates are far below rates that would cause dead-time issues, hence these data in Figure 1 are a good approximation to true pulse-counted data. By way of contrast, Figure 2 is an example of data measured using 0.3 s per data bin and a delay-line-detector operating mode that collects in parallel, multiple distinct data streams. These data streams represent complete spectra offset in energy, which are merged to create the spectrum shown in Figure 2a. Figure 2b shows two energy intervals marked with grey colored zones from the data in Figure 2a fitted with a linear polynomial. The black residual plot at the top of these zones in Figure 2b is analyzed in terms of the intensity of variation relative to these linear approximations to background signal. The frequency of data bins concerning the intensity of variation is displayed as a histogram in Figure 2c. The distribution shape in Figure 2c is consistent with a normal distribution, which is known to approximate a Poisson distribution. Therefore, empirically it is possible to show that XPS data, under the correct circumstances, have noise characteristics for which Equation (1) returns values close to unity.

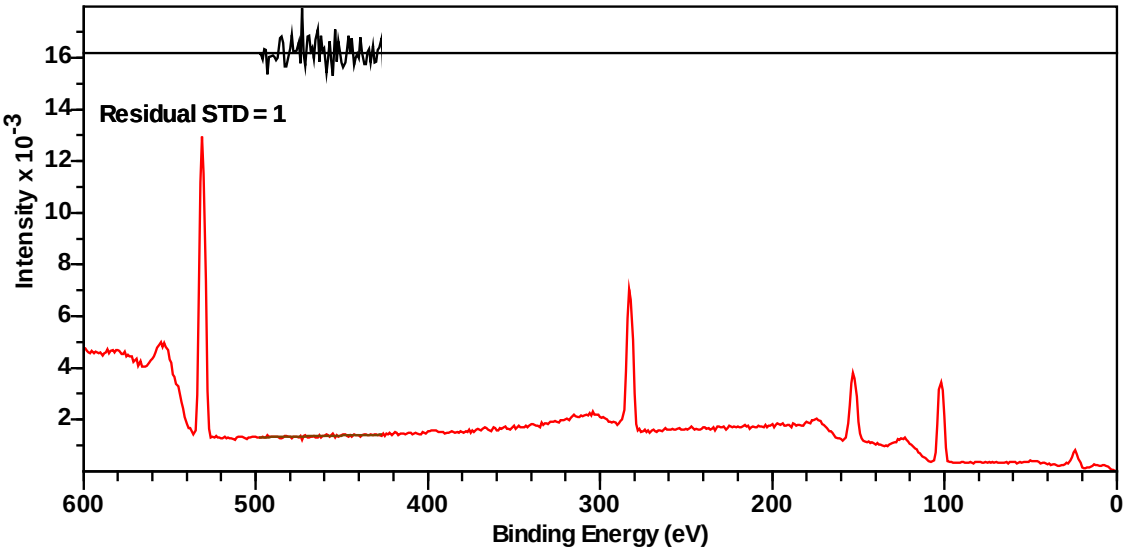

Figure 1. Pulse counted SiO_2 spectrum recorded using a single detector. The two regions marked independently calculate linear polynomials that fit the signal in the least squares sense. The value calculated for the residual STD is unity because electrons were counted using a delay line detector operating as a single detector. Hence, true pulse counting is approximated by these data.

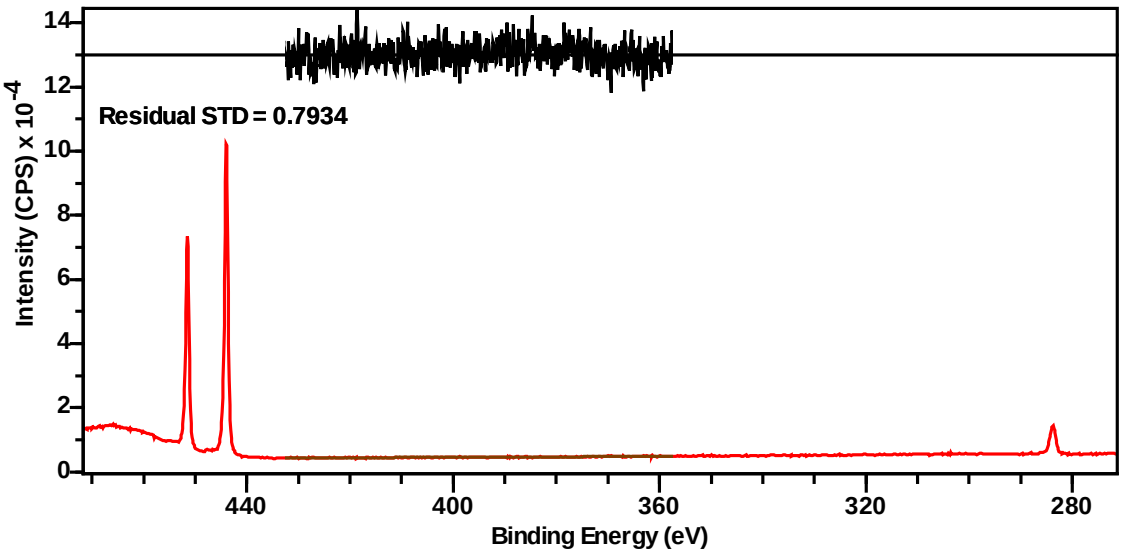

(a)

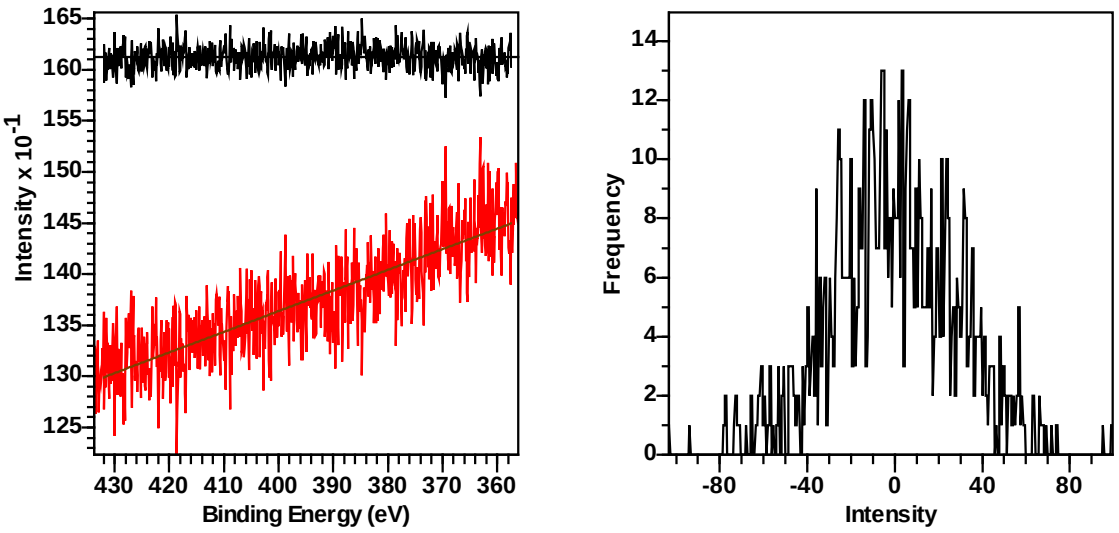

(b) (c)

Figure 2. (a) Spectrum recorded using multiple data streams. The energy interval marked in grey is used to create the results shown in (b) and (c). Note that the residual STD value of 0.79 calculated by fitting a linear polynomial to the inelastic background is less than unity. Merging multiple data streams to form a single spectrum has consequences for noise characteristics in data. The processing of the signal from multiple data streams effectively smooths noise in the computed spectrum. (b) Signal measured during an XPS experiment for a section of inelastic background signal without photoemission resonance peaks. Data are displayed in red, while a linear background and residual plot are colored black (c) A histogram of frequency for deviations in counts per bin from a linear polynomial that fits data in the least squares sense. The fit to data for the computed linear polynomial in (b) creates a residual trace (black) with the distribution of intensity relative to the linear polynomial shown in (b).

Components and Peak Models

A peak model is a set of curves that when summed together creates a single curve that, when correctly adjusted, approximates shapes within spectra. The basic unit used to define a peak model is a component of the peak model, which is a parametric curve that defines the characteristic shape of photoemission data (line-shape) and adjustable parameters used during optimization. The function of the curve defined for a component is to mathematically model the photoemission signal (peak or background signal) using shapes based on physics. Adjustable parameters (FWHM, area and position) are designed to both allow optimization to fit the peak-model curve to data and to allow physical properties to be assigned to a component, such as binding energy or photoemission intensity.

Components and Chemical State

XPS creates spectra by irradiating a sample with photons of given energy causing the emission of electrons. Electrons emitted from the sample are detected over a range of energies which take two forms, namely, electrons that escape the sample without losing energy and electrons that experience inelastic scattering and therefore emerge with energy

different from the initial energy due to photo-ionization. Photoemission due to the scattering of bound state electrons by photons of specific energy is recorded to form an energy spectrum with shapes characteristic of the chemical state. Emission signal from quantized bound states is detected at energies depending on the binding energy of core level electrons scattered by photons and concentrate signal over a narrow energy interval compared to broad structures typical of background signal. Spectra contain peak shapes that result from primary emission (photoelectron) due to scattering of core-level electrons and secondary emission in the form of Auger electrons. The latter has kinetic energy that is independent of photon energy, but primary emission results in electrons with a kinetic energy that depends on both the core level involved and the energy of the photon. The dependence of primary-photoemission kinetic energy on photon-energy is the reason XPS spectra are presented as intensity plotted against binding energy. Binding energies from core level electron configurations tend to be emitted with significant differences in energy for different core levels, however, the exact binding energy for a core level electron within an atom depends on the chemical bonds between the atom and other atoms in the sample. Thus, when C 1s for example is measured from a material known, such as Nylon, rather than a single photoelectron peak, the spectrum for C 1s photoemission shown in Figure 3a is the sum of several peaks, each offset in energy due to carbon bonded to other carbon, hydrogen, nitrogen and oxygen (Figure 3b).

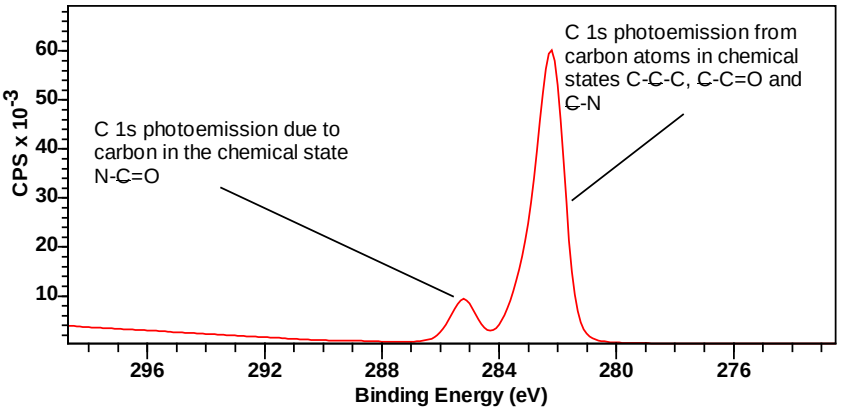

(a)

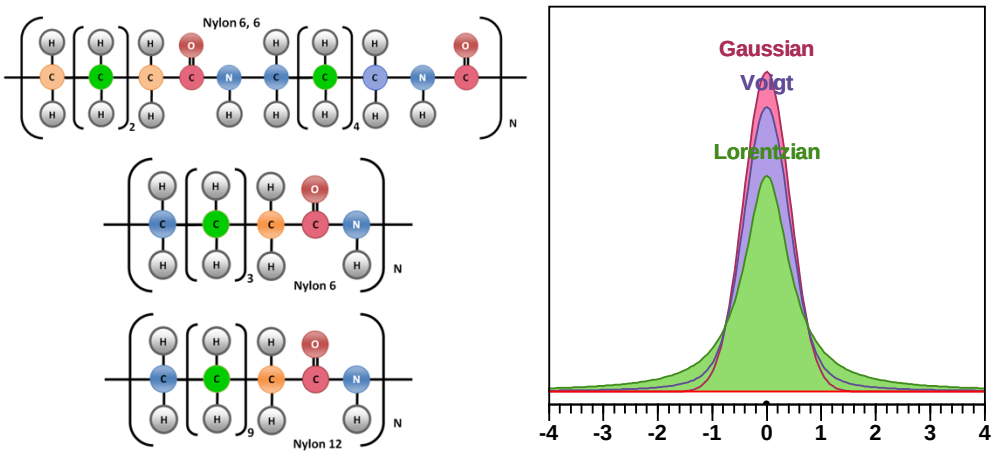

(b) (c)

Figure 3. (a) C 1s spectrum measured from a sample described as Nylon. (b) Three possible chemistries for materials nominally described as Nylon. Carbon appears in the four chemical states N-C=O (red), C-N (blue), C-C=O (orange) and C-C-C (green). For Nylon 6,6 and Nylon 6 the proportions for these chemical states are 1:1:1:3, while for Nylon 12 the proportions are 1:1:1:9, respectively. (c) Examples of bell-shaped curves suitable for modelling photoemission signal.

One of the advantages of XPS as an analytical technique is it is possible to identify photoelectron peaks shown in Figure 3a with chemical interpretations for these peaks as illustrated in Figure 3b. Figure 3a demonstrates two features of the XPS signal. Firstly, provided data are acquired with sufficient energy resolution, it is possible to see different chemical states for carbon atoms in Nylon (illustrated for N-C=O chemistry compared to other chemistry for carbon in Nylon). Secondly, the only photoemission peak easily identified in Figure 3a is N-C=O (red). The other three chemical states (color-coded in Figure 3b) for carbon in Nylon (C-C-C (green), C-N (blue) and C-C=O (orange)) involve correlated signals and therefore, investigating the chemical state for Nylon requires the use of a peak model.

Bell-Shaped Components and XPS

Examples of commonly used functional forms with the characteristics of bell-shaped curves are illustrated in Figure 3c. These three mathematically defined shapes are plotted in Figure 3c, where the areas bounded by the curves and the x-axis for all three are identical and all are defined with the same full width and half maximum (FWHM). Bell-shaped curves used in XPS are often constructed from two easily defined mathematical functions, Equation (5) and Equation (6). The natural line shapes for photoemission are assumed to be close to the Lorentzian shape in Equation (5) illustrated in Figure 3c. However, observed line shapes tend to appear with characteristics that differ from a pure Lorentzian shape. To accommodate these shapes in observed line shapes a Gaussian (Equation (6)) is blended mathematically with a Lorentzian, such as performed through a convolution integral (Equation (8)). The convolutions in the form of Equation (8) reduce to a Voigt function for the case where α and β in Equation (7) are both set to unity. A Voigt function is symmetrical, however, XPS data

can involve asymmetric line shapes. Therefore, the line shape in Equation (8) makes use of the generalized Lorentzian in Equation (7) to offer a means of introducing asymmetry into a line shape. Pseudo-Voigt line shapes often appear in the literature for historical and practical reasons. These pseudo-Voigt functions are defined in the form GL(m) or SGL(m), where the parameter m ranges over an interval [0,100], for example, such that m=0 corresponds to a pure Gaussian and m=100 corresponds to a pure Lorentzian. To mimic GL(m) and SGL(m) definitions in a Voigt function, the LA(m) line shape defined by Equation (9) fulfils this role, subject to the limitation of performing the convolution integral in Equation (8) by numerical means. The value 1401 used in Equation (9) is an arbitrary number used to define the upper limit to the width of a Gaussian used in Equation (8), hence LA(0) is not a pure Gaussian

$$Lorentzian\colon l(x) = \frac{1}{1+4x^2} \quad (5),$$

$$Gaussian\colon g(x) = e^{-4ln2x^2} \quad (6).$$

Voigt line shapes are defined from Lorentzian and Gaussian functions via the special case of a generalized Lorentzian (Equation (7)) and the convolution integral in Equation (8)

$$Generalised\ Lorentzian\colon l_g(x\colon \alpha,\beta) = \begin{cases} [(l(x)]^{\alpha} & x \leq 0 \\ [l(x)]^{\beta} & x > 0 \end{cases} \quad (7)$$

$$Lineshape\colon LA(x\colon \alpha,\beta,n) = N\int_{-\infty}^{\infty} l_g(\tau\colon \alpha,\beta)g(x-\tau\colon f_G(n))d\tau \quad (8).$$

The symmetric line shape $LA(x,m)$ specified by the string LA(m) is constructed from the definition for $LA(x\colon \alpha,\beta,n)$ and the maximum allowed value n defining the width for the Gaussian term in the LA convolution integral in Equation (8)

$$LA(x,m) = LA\left(x\colon 1,1,\left(1401-\left(\frac{m}{100}\right)1401\right)\right) \quad (9).$$

The analysis of spectra by fitting curves to data is often seen as synonymous with fitting bell-shaped curves to data. In the case of Nylon, there is a strong case for following this model of defining chemical state signal from C 1s photoemission using individual bell-shaped curves. However, there are many examples in XPS data where the chemical state in an atom induces complex shapes that do not lend themselves to the paradigm of one bell-shaped curve for one chemical state. Metal oxides, for example often manifest as sequences of peak structures all coalesce to form a data envelope that characterizes specific oxidation states of a metal.[10,11] While one should be aware of the limitations of assuming one bell-shaped curve for one chemical state, an analysis of Nylon making use of a peak model constructed from four component curves (each representing a different chemical state of carbon) provides talking points of significance to anyone new to the use of peak models in XPS and optimization that fits peak models to data.

Background Curves

The peak models presented in this manuscript make use of components that model background signals. The Shirley algorithm[12] applied to a bell-shaped line shape provides a sigmoid response that can be positioned appropriately to account for the inelastic scattering

of electrons for a material with a threshold limit for energy loss (see V4 in supplementary material for explanation on Shirley type background).

For any synthetic line shape $F(x)$ a Shirley profile line shape is computed using the integral in Equation (10). The notation in Equation (10) is designed to allow the use of any line shape to be used to create a component with Shirley's shape. For example, Equation (10) would apply equally well to pseudo-Voigt functions GL(m) and SGL(m) by creating sigmoid type curves defined by SB(0)GL(m) or SB(0)SGL(m).

$$SB(0)F(x) = \int_x^\infty F(\varphi)d\varphi \quad (10).$$

The sigmoid shape defined by Equation (10) may be defined as a component of a peak model. Since a curve based on Equation (10) involves the integration of a parametric curve in the form of a bell-shaped curve, the energy for the sigmoid-shaped component in a peak model is determined by the energy for the bell-shaped curve appearing in the integral. Thus, the sigmoid shape may appear at any energy determined by the optimization algorithm that fits the peak model to data.

A sigmoid shape constructed from Equation (10) is applied directly to data, where a basic linear background is first removed from data, similarly providing the basis for constructing a background for Nylon. The Shirley background shape initially computed can be offset in energy and therefore provides a linear background augmented with a Shirley sigmoid shape calculated from data that models a rise in background intensity in response to a photoemission peak at energy different from the peak itself.

An alternative approach to constructing a background curve shape is the use of a background described as a three-parameter universal cross-section Tougaard background[11,13] defined by Equation (11) and Equation (12). The background $T(E)$ is computed from the measured spectrum $J(E)$, representing the photoelectron peak plus signal due to inelastic scattering of these photoelectrons by electrons within the sample, using the integral:

$$T(E) = \int_E^\infty F(E' - E)J(E')dE' \quad (11).$$

The integral is constructed by making use of information in the form of the Tougaard Universal Cross-Section that provides a means of modifying background signal in response to the material properties of a sample. These material properties are input via cross-section parameters C, D and T_0 defined in Equation (12).

$$F(x) = U(x: B, C, D, T_0) = \begin{cases} \frac{Bx}{(C-x^2)^2+Dx^2} & x > T_0 \\ 0 & x \leq T_0 \end{cases} \quad (12)$$

For as-measured spectra, the B parameter is used to scale the background curve concerning intensity at some kinetic energy lower than the photoemission peak for which a background is required. The more powerful aspect of the Tougaard approach is the cross-section, which when available provides informed guidance for shapes within the background signal. These parameters are not arbitrary and must be determined on physical grounds for specific

materials. Tougaard published examples of backgrounds based on Equation (11) and Equation (12), one of which is a prescription for use with general polymer spectra. The Tougaard approach to computing background signals is designed to model extrinsic background shapes. That is, shapes in background signal that are a consequence of inelastic scattering of photoelectrons following excitation to the continuum states for the atom from which photoionisation occurs. Of particular interest for Nylon spectra is the parameter in Equation (12), namely, T_0 which is intended to delay the onset of the background signal concerning a photoemission peak. Thus, the role of the T_0 the parameter is to model background shapes via Tougaard backgrounds constructed for insulating materials, which is similar to the logic of using a Shirley sigmoid-shape offset in energy from the photoemission peak in question.

Introducing the Tougaard background is done to provide the context for modelling the background in Nylon using Shirley-type backgrounds. Specifically, Tougaard backgrounds are designed to account for inelastic background response to a photoemission peak for many-electron volts to lower the kinetic energy of the photoemission peak. The same is difficult to justify for backgrounds based on Shirley's approximations. The use of a sigmoid shape derived from the Shirley algorithm is only plausible in the case of Nylon at the point the background signal first responds to photoelectrons from a given Nylon core level. In the case of modelling C 1s spectra, the following section justifies the use of a sigmoid background approximation, which is used predominantly to allow for a specific Voigt line shape used for N-C=O photoemission. The interaction of background curves and line shapes used to model photoemission is never easy to scientifically justify, but the use of line shapes with greater Lorentzian character does require some accommodation in background curves and these aspects of XPS data analysis are the motivation to illustrate through Nylon how the line shape selection makes a difference to background selection and ultimately the outcomes to physically meaningful parameters when fitting peak models to data.

Discussion and Results

Goodness-of-fit statistics are only meaningful if a peak model accurately represents the chemistry in a sample. It is relatively easy to create a peak model that fits data with fitting statistics compatible with pulse-counted data. Simply adding components to a peak model and performing optimization without constraints will ultimately permit high-quality data reproduction, but will fail to provide physically useful information about a sample. The case considered in this manuscript is where a peak model represents chemistry in Nylon, but when fitted to data, the fitting statistics are suboptimal concerning fitting statistics for a perfect peak model applied to true pulse-counted data. These peak models with suboptimal fitting statistics still provide useful information about sample composition because of the logic used to construct these peak models. An explanation of the logic used to create peak models, based on sample knowledge, awareness of instrumental factors and awareness of data-analysis limitations/strengths, helps to allow others in accepting results from XPS when offered with suboptimal fitting statistics. Hence, the following provides details for the process by which peak models are constructed and applied to data measured from Nylon samples.

Survey Interpretation

The most crucial step in modelling photoemission data is determining the number of component curves used to describe the chemistry of the sample. When presented with data such as that shown in Figure 3a and the statement that the sample is Nylon, the temptation is to settle on four chemical states for carbon atoms as shown in Figure 3b. However, even for a sample of known origin, it is advisable to measure a survey spectrum before attempting to understand a narrow scan spectrum in isolation. A survey spectrum offers information about two basic aspects of the sample. Firstly, a survey allows an investigation of what else might be within a sample that might influence shapes for signals within a narrow scan C 1s spectrum. Secondly, survey data are often measured using operating modes for an instrument that allows relative intensities for photoemission peaks to be interpreted as the amount of substance. Nylon is nominally a bulk homogeneous sample. Accurate elemental quantification by XPS is only possible under special circumstances (homogeneous materials and well-calibrated instrumentation),[14] nevertheless, measuring photoemission peak intensities as a percentage of signal from different atoms (even for samples which do not conform to the cases for which XPS can be interpreted as amount-of-substance) provides information useful in constructing a peak model. That is, if the survey quantification results in unexpected proportions for elements in a sample, attempting to understand the reasons for these results provides food for thought used in building a peak model. For example, an excess of carbon compared to nitrogen and oxygen in a material assumed to be Nylon requires explanation and might explain anomalous proportions for components in a peak model when fitted to C 1s data. The survey spectrum corresponding to the C 1s spectrum in Figure 3a is shown in Figure 4. A quantification table calculated from integration regions is displayed in Figure 4 which suggests there is an excess of carbon for Nylon 6 or Nylon 6,6 but insufficient carbon if the sample corresponds to Nylon 12 (Figure 3b). Thus, quantification based on the survey spectrum implies a peak model for Nylon which is formed from four component peaks in proportions expected for Nylon (3:1:1:1), may not fit these data in Figure 3a with fitting statistics of sufficient quality to have confidence in the results from the fit to data.

While a Nylon sample may be presented for analysis as a bulk material, in practice XPS may have a different interpretation for sample composition. Quantification by XPS as shown in Figure 4 (and in general) is difficult to interpret owing to the surface sensitivity of the technique. That is, the XPS signal after subtraction of inelastically scattered background derives from the top three attenuation lengths of the sample. For Al anode X-ray sources, the volume of material sampled is less than 10 nm. Therefore, unless the sample is perfectly homogeneous the volume sampled does not represent the chemistry of the bulk material. A sample that might be considered homogeneous in the bulk may have surface contamination or differences in composition localized to the surface interface that biases quantification results. Hence, while the survey spectrum in Figure 4 implies an unexpected carbon contribution, due to uncertainties in quantification by XPS, these results should be seen as a guide rather than entirely accurate. The energy resolution of these survey data is insufficient to identify the nature of the excess carbon concerning Nylon 6. Therefore, to make progress in understanding data in Figure 3a a peak model is required, but a peak

model that does not precisely match the expectation for relative component area implied by Nylon, but also, does not necessarily match exactly the amount of excess carbon determined from survey data.

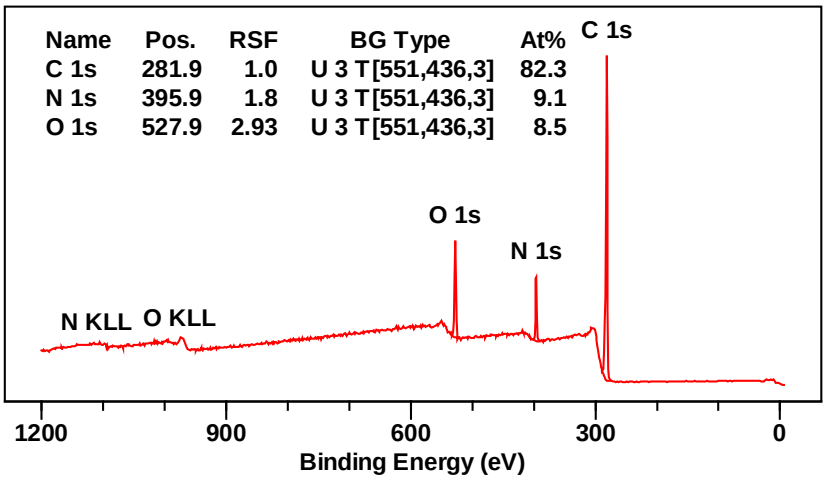

Figure 4. Survey spectrum measured using pass energy 160 eV operating with lens mode FoV1. Quantification tabulated over the survey spectrum is performed using removal of background signal by a Tougaard approach and correction factors, specific to this measurement, that convert intensity to amount of substance. Scofield cross-sections are the source for RSFs which are corrected for escape depth. FoV1 is an imaging mode for the Kratos Axis Ultra XPS instrument and when tuned to create registered images of the sample of the constant area the intensity response of FoV1 to changes in kinetic energy is relatively flat over a wide range of energies. Hence quantification based on Scofield cross-sections and escape depth correction without the use of the Kratos transmission yields results for atomic concentration that are expected to be reasonably accurate. The table of atomic percentages computed from integration regions defined for C 1s, N 1s and O 1s photoemission suggests an excess of carbon compared to both nitrogen and oxygen. Background approximations for these regions are consistently applied to each photoemission peak using Tougaard universal cross-section parameters constructed for general polymer materials.

Estimating Background Curves for Nylon

The background signal is generally the result of electrons that are initially emitted from atoms with kinetic energy higher than the photoemission peak under analysis. However, changes to the shape of the background signal beneath a photoemission peak are the result of inelastic scattering of photoelectrons from the peak in question. While a response in the background signal to the photoemission peak is observed for certain materials (most notably metals), for Nylon an immediate response in the background to the photoemission peak does not occur. For inelastic scattering to occur electrons in states for which scattering is allowed by quantum mechanics must be available. One of the characteristics of insulator materials is that the inelastic scattering of photoelectrons is offset in energy from the energy for the photoemission peak representing a zero-loss energy signal. In practical terms, the background signal beneath Nylon peaks follows the general trend in the background, which is readily approximated by a linear polynomial. However, in the case of C 1s emission

from Nylon, chemically shifted photoemission from different bond states for carbon is spread over an interval in energy in which a Shirley response is possible. These energy offsets in the response of the background to a photoemission peak are material-dependent and therefore need assessing for Nylon photoemission. Chemical shifts for the C 1s signal illustrated in Figure 3a make it difficult to see the influence on the background due to the inelastic scattering of C 1s photoelectrons. However, in the case of Nylon, estimates for the characteristic energy-offset to background signal underneath a C 1s signal can be obtained by considering N 1s and O 1s spectra. Both N 1s and O 1s photoemission from Nylon is the result of single chemical environments for N and O with distinct binding energies for 1s electrons. Therefore, photoemission for N 1s and O 1s yields one photoemission peak per element that is well resolved from any interfering emission. Figure 5a and Figure 5b present an analysis of the background response to O 1s and N 1s photoemission, respectively. These photoemission peaks are sufficiently narrow and the background response to these photoemission peaks is offset in energy enough to allow an estimate to be established. Given the estimate in Figure 5a and Figure 5b for the energy offset for N 1s and O 1s (6.9 eV and 5.6 eV, respectively), a reasonable estimate can be made for a similar response in background signal to C 1s photoemission (Figure 5c). Specifically, the energy offset in background response for C 1s photoemission occurs to slightly higher binding energy than the component representing C 1s N-C=O emission. Thus, the set of four bell-shaped curves used to model C 1s chemical state in Figure 5c are arranged on a flat background, an assumption also supported by the relatively flat shape of background signal at lower binding energy to C 1s visible within survey data in Figure 4.

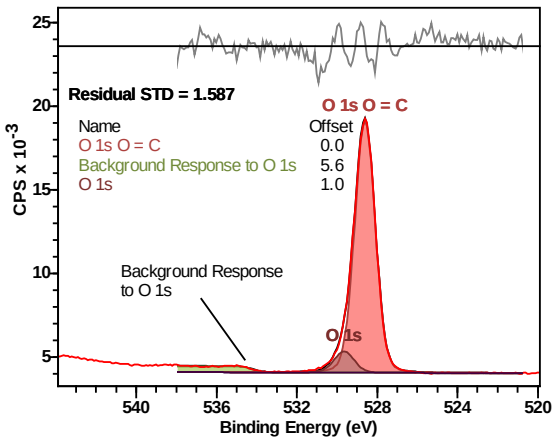

(a)

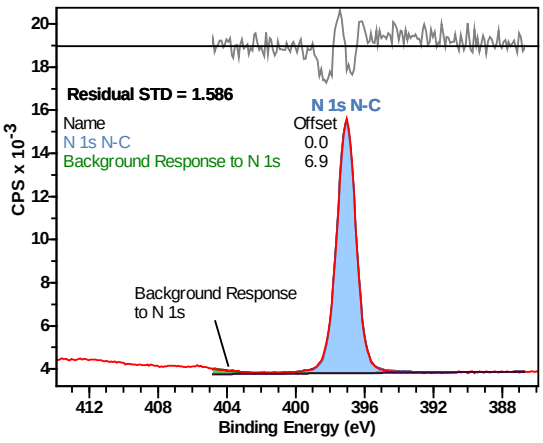

(b)

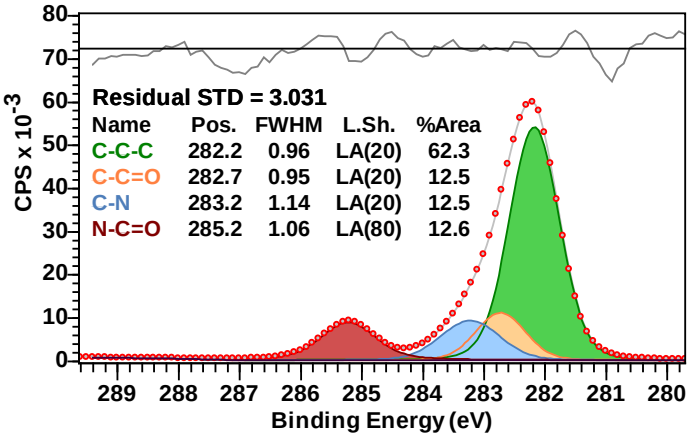

(c)

Figure 5 (a) O 1s photoemission measured from Nylon using dwell-time of 200 ms and 33 scans. A linear background is extrapolated from a fit of a linear polynomial to data with lower binding energy than the O 1s photoemission peak. A sigmoid curve computed from the O 1s O=C component is included in optimization when the peak model is fitted to O 1s data. The difference in energy between the position for the sigmoid background component and the component representing O 1s photoemission with chemical state O=C is 5.6 eV. (b) N 1s photoemission measured from Nylon using dwell-time of 200 ms and 33 scans. A similar analysis to that performed on O 1s applied to N 1s demonstrates that the background response to N 1s photoemission is offset to higher binding energy by about 6.9 eV. In the case of N 1s, the background response is less well defined than O 1s resulting in a sigmoid component with an FWHM of 1.6 eV compared to the FWHM for the corresponding sigmoid component of 0.52 eV, hence there is greater uncertainty in the offset in energy computed for N 1s photoemission.

Bell-Shaped Components in a Nylon Peak Model

The peak model in Figure 5c is constructed assuming the chemistry for carbon shown in Figure 3b, namely, carbon appears in Nylon bonded to (1) carbon and hydrogen (C-C-C), (2) bonded to carbon where carbon is perturbed in energy due to a bond to carbon that is also double bonded to oxygen (C-C=O), (3) nitrogen (C-N) and (4) double bonded to oxygen (N-C=O). Each peak in intensity from carbon atoms bonded to atoms as listed is offset in energy, therefore four components to the Nylon peak model in Figure 5c are arranged with binding energy reflecting these chemical states of carbon and the components representing these chemical states have FWHM and intensity (measured by area CPSeV) that suggest relationships between carbon, oxygen and nitrogen from which the relative numbers for these atoms within the sample can be estimated. Before considering the information about the sample implied by the peak model in Figure 5c, the justification for the peak model is explained below.

Components for a Nylon Peak Model

The primary motivation for selecting four components for the peak model in Figure 5c is the expected chemistry of Nylon as shown in Figure 3b. The caveat for the peak model in Figure

5c is that the intensity ratio for carbon in the four chemical states as shown does not agree with the idealized relationships illustrated in Figure 3b. The component corresponding to CH_2 bonded to CH_2 only (C-C-C) concerning other carbon atoms in the differing chemical state, should be on average, either 3:1 (Nylon 6 or Nylon 6,6) or 9:1 (Nylon 12). The same ratio determined based on the peak model in Figure 5c is 5:1. Quantification for this sample based on integration regions and survey data similarly suggests an excess of carbon for Nylon 6 or Nylon 6,6. Results from both the peak model in Figure 5c and the survey spectrum in Figure 4 agree that the amount of carbon atoms is unexpected for Nylon depicted in Figure 3b. However, assuming the peak model in Figure 5c is correct, then the peak model provides information about carbon not available from the survey data, namely, the excess carbon appears to be of the form CH_2 bonded to CH_2 only. Such an observation would indicate the sample includes significant contamination with adventitious carbon or the termination of this particular form of Nylon, at the interface to the vacuum, favors collecting of signal from CH_2 bonded to CH_2 only preferentially over the other three chemical states for carbon. Before concluding excess CH_2-CH_2 is the source of excess carbon a review of FWHM for component peaks is required and how the constraints in the peak model influence the outcome for optimization.

Full Width at Half Maximum

The width of a photoemission peak is a result of several factors that involve instrumental, sample and the photoemission process. At a fundamental level, the shape of a photoemission peak is determined by uncertainty in the energy for electrons in an atom when scattered by a photon. If it were possible to measure a photoemission line without other factors then the natural line shape and width for that line would be the lower limit to the FWHM for the measured photoemission signal. In the case of photoemission due to scattering of C 1s electrons in carbon, a range of line shapes and FWHM are observed in spectra, as measured, because of uncertainty in energy introduced by instrumental factors involving transporting electrons emitted from the sample to the detectors as shown in Figure 6a. These detectors are positioned to record electrons after traversing an energy filter. The arrangement of these detectors concerning the energy-filter exit-plane permits energy to be assigned to an event occurring at each detector. Uncertainty in energy for an electron is introduced through interpreting a position for a detector as energy for an electron and the distribution of electron energies that are accepted by a detector. The response of the sample to the emission of an electron also introduces uncertainty in the energy of electrons counted by instrumentation. When considering what FWHM should be expected for a photoemission line as recorded for C 1s, examining spectra using different instrument modes and samples allows an informed decision to be made for a target FWHM. C 1s spectra from Nylon using different energy resolutions for the energy filter with better energy resolution than the spectrum in Figure 5c yield similar width components to those in Figure 5c. Thus, the FWHM for C 1s photoemission from Nylon is not limited to any significant degree by the energy resolution of the instrumental mode used to collect these data. The logic underpinning this assertion is now described.

The role played by instrumentation (see V5 and V6 in supplementary materials for operating modes of XPS including scanning mode, pass energy and energy resolution) in observed

FWHM is more important the narrower the natural width for a photoemission line. In the case of carbon, the narrowest of commonly studied photoemission lines is obtained for graphite. To understand how instrumentation alters FWHM for C 1s photoemission, experiments performed for a graphite sample using different operating modes create the same natural line shape a series of recorded shapes. Two factors that alter the recorded line shape for an XPS instrument are the energy filter pass energy (PE) and the dimension and influence of apertures within the lens column that transfers electrons from the sample to the detectors. To illustrate the role played by instrumentation on FWHM, C 1s spectra are recorded from graphite using two PEs and two aperture settings (Figure 6b and Figure 6c). Aspects of an XPS instrument relevant to energy resolution and therefore FWHM are now presented.

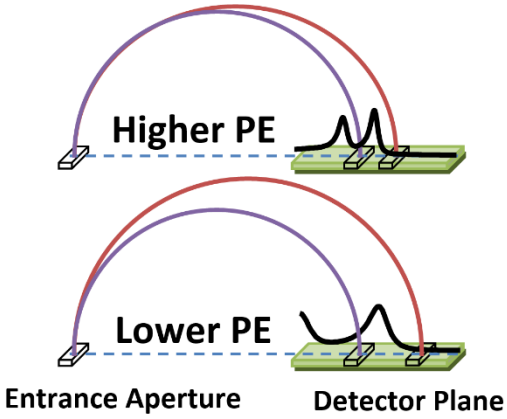

(a)

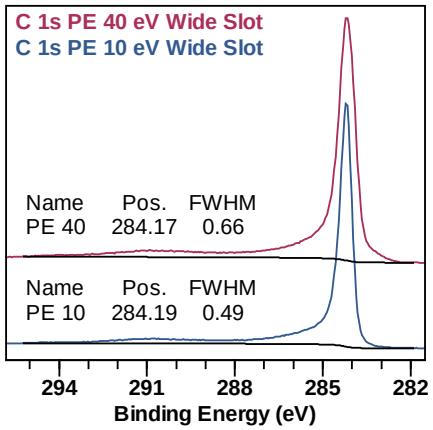

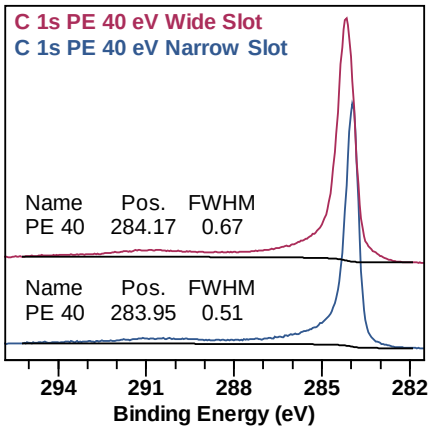

(b) (c)

Figure 6. (a) Illustration of how the pass energy and aperture widths influence energy resolution for spectra and therefore FWHM for measured photoemission peaks. The inner arc colored blue represents the trajectory for an electron with kinetic energy equal to the PE for an HSA. The outer trajectory colored red represents the trajectory for an electron with kinetic energy higher than the PE. (b) C 1s spectra measured from graphite powder sample using PE 40 eV and PE 10 eV using the same default slot aperture referred to as Wide Slot. (c) C 1s spectra measured from graphite powder sample using PE 40 eV measured using two

different aperture widths. The spectrum labelled C 1s PE 40 eV Wide Slot is measured using the same operating mode as PE 40 eV data in (b). The spectrum labelled C 1s PE 40 eV Narrow Slot makes use of a custom selected area aperture to project an image into the entrance aperture for the HSA which is of width approximately one quarter the width of the default slot selected area aperture for a Kratos Nova Axis at University of Nantes, France. Note that in both (b) and (c) by either lowering the PE or reducing the width of the effective aperture for electrons entering the HSA, both result in narrower FWHM than PE 40 using the Wide Slot aperture.

The term pass energy in the context of XPS refers to the energy of an electron entering the energy filter (most commonly a hemispherical analyzer (HSA)) with a direction parallel to the axis of symmetry for the energy filter, follows a circular path from the entrance plane to the HSA to the exit plane (Figure 6a). The strength of the electric field between two concentric hemispherical electrodes of an HSA determines the energy that passes an electron from the entrance to the exit of the HSA. Energy filtering for electrons of different kinetic energies to the PE follows trajectories that disperse in position the point of exit at the detector plane to the HSA (Figure 6a). Thus, by placing apertures at the entrance to the HSA, a degree of control is achieved for electron trajectories allowed to pass through the energy filter. Apertures at the exit to the HSA allow electrons with these limited trajectories (imposed by the entrance aperture and electric fields) to leave the energy filter and therefore are made available for detection. Hence a combination of PE and aperture widths influence the uncertainty in energy for electrons detected with energies close to the PE for an experiment. The lower the PE the weaker are forces acting on electrons and therefore, for electrons with different energies, the greater the dispersion in position at the exit aperture (Figure 6a). Less obvious is the role played by aperture widths to photoemission peak widths. At the heart of the physics involved in the energy filtering of electrons are the electron-optical properties of the lens column that transfers electrons from the sample to the detector. Electrons from the sample enter the HSA using lenses forming an image at the entrance to the HSA. The image formed may be that of an illuminated entrance aperture or an image focused by the electron optics to a specific size, but regardless of how this image is formed, the HSA transfers the image at the entrance to the HSA to the HSA exit plane with a magnification of -1 with the image dispersed in position depending on the energy of electrons entering the HSA (Figure 6a). Apertures at the HSA exit plane, either physically arranged or logically implemented through detector partitioning, determine the uncertainty in energy for electrons detected. The uncertainty in energy for an electron is a result of the confusion between image size and numerous images formed at the detector plane for electrons with energies different from the PE. Lowering the pass energy reduces the uncertainty in energy by dispersing images with differing energies to a greater degree and/or reducing the entrance aperture width to reduce the size of the image in the energy dispersive direction at the HSA exit plane. Therefore, lowering PE and/or reducing aperture widths reduces the confusion between positional information and energy information for an electron when detected. These instrumental factors influencing the FWHM for measured photoemission peaks are illustrated using C 1s spectra measured from graphite. Figure 6b

compares C 1s spectra measured from graphite using PE 40 eV and PE 10 eV. Figure 6c compares C 1s spectra measured using the same PE 40 eV with different aperture widths for the image formed at the entrance plane to the HSA.

There are two points worth noting from Figure 6 relating to Nylon components. Firstly, C 1s measured from graphite have FWHM for PE 40 eV Wide Slot is estimated to be 0.66 eV. Therefore, it is unlikely that any component representing C 1s has FWHM below 0.66 eV. Since the components used in Figure 5c for Nylon are all close to unity, the implication is that the FWHM for components representing Nylon chemistry is limited in FWHM by the sample rather than the instrument energy resolution. The second point worth highlighting in Figure 6c specifically is that the apparent binding energy for graphite is not identical between PE 40 eV measured using different widths for the slot aperture. The difference in apparent binding energy between a wide and a narrow slot is mostly due to the position of the narrow slot within the entrance aperture to the HSA. The position of the narrow slot image within the entrance slot alters the trajectory for electrons within the HSA resulting in a different position at the exit plane and therefore measured energy. This observation regarding the position of the narrow slot image within the entrance aperture to the HSA, to some extent, explains why the line shape for C 1s measured from graphite is less well formed when a wide slot aperture is used compared to a narrow slot aperture. The wide slot aperture is effectively the sum of narrow slot apertures with images concatenated to form a tessellation of the wide slot. Each such narrow slot, so defined, creates independently C 1s data with the energy resolution shown for the narrow slot aperture in Figure 6c, but each spectrum with FWHM close to 0.51 eV is offset in energy due to the offset in narrow slot images required to form the tessellation as described. Thus, the FWHM for C 1s was measured using PE 40 eV and the wide slot aperture is 0.67 eV. Similarly, the line shape for PE 40 Wide Slot aperture is less representative of the natural line shape than if lower PEs are used or a narrower slot aperture is available. The disadvantage of better resolution data is a lower signal to noise for the same acquisition time. It is clear from Figure 6 that shapes in C 1s spectra are influenced systematically by instrumental factors. However, since the Nylon sample as measured yields components with FWHM close to unity, the instrumental factors highlighted by graphite are of lesser importance to line shapes for Nylon. Nonetheless, these instrumental factors exist and deform natural line shapes, albeit to a lesser extent, a consequence of which is that extended measurement times amplify these instrumental shapes relative to random noise. Thus, one explanation for the figure-of-merit for the Nylon peak model in Figure 5c is the extended period used to measure these data, causing non-chemical systematic shapes, that are difficult to reproduce mathematically in line shapes, to overwhelm pulse counting noise. When temporal influences are coupled with imprecise line shapes, this results in the residual STD statistic of 3 rather than unity. The following text expands on the nature of systematic shapes in Nylon C 1s spectra and how the choice of line shapes alters outcomes to optimization.

Specifics of Line Shapes used in Nylon Peak Models

As described above, FWHM for components in a peak model representing the types of chemistry in Nylon is expected to be close to unity. The component table shown in Figure 5c shows all components are close to unity, however, there is a subtlety in these results worth

noting. Line shapes used in Figure 5c are Voigt functions where three components make use of LA(20) while the component representing N-C=O uses the line shape LA(80). FWHM reported in Figure 5c corresponds to a parameter determined during optimization, but FWHM for components with differing line shapes depend to a lesser extent on the line shape, but the area for a component depends on line shape to a greater extent. The dependence of area on line shape can be understood by considering different measures for the width of a line shape. Specifically, the width measured at different heights within a component differs to a greater extent when moving from the line shape LA(20) to LA(80). Figure 7 plots two components in the Nylon peak model adjusted in the component area to be identical and both have identical FWHM fitting parameters. The height difference can be seen in Figure 7, but if the width is measured at different heights below the component maximum, one-half (FWHM), fifth and one-twelfth of the component height, then it is more obvious how changing the line shape alters measured area and width of the signal. The fact that Figure 5c makes use of the line shape LA(80) for the N-C=O signal is significant because underlying the use of LA(80) rather than LA(20), the difference in line shape contributes to fitting data from Nylon using three components of equal area. Beamson and Briggs fit four components in peak models to various forms of Nylon[5,15] with the result that N-C=O signal intensity is lower than C-C-C, C-N and C-C=O. Line shapes and also background curves may be part of the cause for these differences reported by Beamson and Briggs, but the fit shown in Figure 5c is achieved for the given area constraints because of these different line shapes. A further point worth considering relating to Figure 5c is the quality of fit measured by residual STD and the appearance of the residual plot.

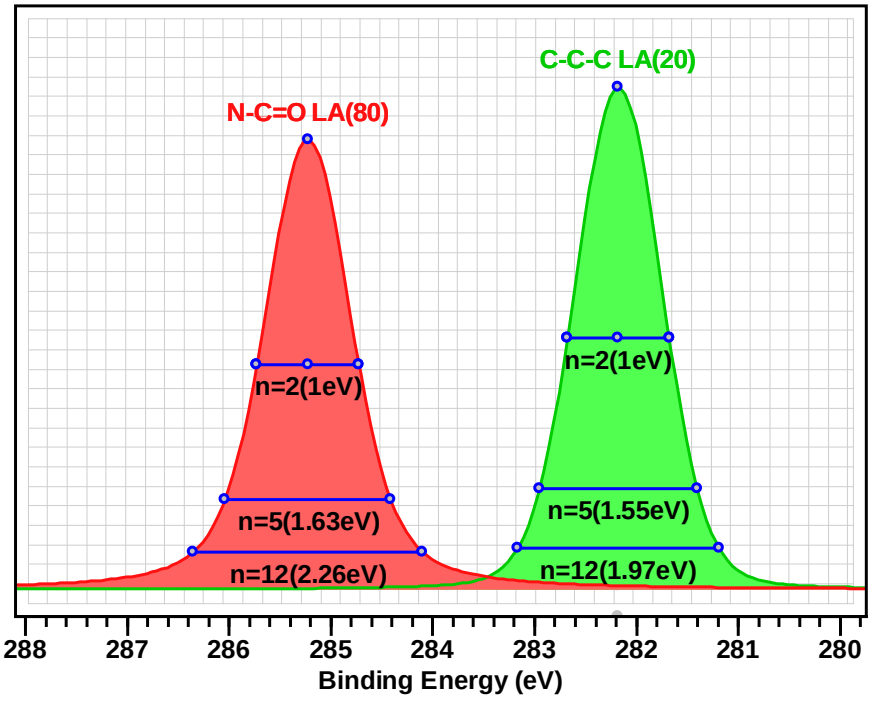

Figure 7. Widths for component peaks with line shapes LA(80) and LA(20) are defined for three heights corresponding to half height (n=2), one-fifth height (n=5) and one-twelfth

height (n=12). Both components are created with an identical area. Note how the same component area L(80) is lower in height than the component with line shape LA(20).

Data Sets Designed for Evaluating Fitting Statistics

Constructing a peak model based on one spectrum is always open to criticism. A spectrum in isolation may, in the worst-case scenario, contain artefacts from the measurement process which may not be obvious by examining one spectrum. There is always the possibility a single spectrum when measured includes shapes unrepresentative of chemistry, simply because the measurement was compromised in some way by operational issues with an instrument. In particular, for insulating samples stability of charge compensation should be proved rather than assumed. Hence repetitions of measurements are an important first step to ensure spectral shapes are repeatable and results extracted from fitting peak models to data are reproducible.

Ideally, an independent researcher should be able to reproduce results obtained through analysis of material by similar measurements and similar data treatment. In practice, different instruments and different operating modes may result in changes to the recorded shapes of photoemission peaks as well as background signals. Thus, a peak model may require modifications before application to spectra from a different source. Nevertheless, the objective of creating a peak model is to make use of background curves and bell-shaped curves that are robust in the sense the same peak model can be applied to similar data through justifiable minor adjustments to curves that represent shapes in the signal. With this aim in mind, constructing a peak model is explained in this manuscript based on data measured using two different approaches. These two different approaches to the acquisition of data are now described.

The spectrum in Figure 3a is acquired as part of an experiment in which O 1s, N 1s, C 1s and valence band data are acquired using the dwell-time per data bin equal to 200 ms, but where each spectrum is accumulated over 33 scans before moving in energy to the next spectral region. The second approach involves spectra measured using the same dwell-time of 200 ms per data bin, however, in this experiment each spectrum for O 1s, N 1s, C 1s and valence band is recorded and saved separately for 33 cycles of measurements over these four spectral energy intervals. These two data sets, therefore, measure each spectral region with equal total acquisition time, however in one case the 33 separate C 1s spectra with lower signal-to-noise are available whereas in the other case one C 1s spectrum with good signal-to-noise is the result. The motivation for measuring Nylon spectra by these two means is to monitor how fitting statistics obtained for a peak model change with dwell time per data bin. Therefore, a peak model is designed to fit chemically meaningful shapes in Nylon spectra. Shapes in data that are not chemically meaning full should not alter the fit to data and are described as noise. Noise in XPS data is not limited to the statistical uncertainty in pulse-counted data. Systematic noise is also a feature of measured data, that is not modelled by Poisson statistics. These measurements are designed to highlight systematic noise in spectra. When considering noise in spectra, the benefit of measuring data by these two means is that a peak model developed for C 1s can be evaluated against data with different combinations of noise due to pulse counting and instrumental noise. The influence

of these two types of uncertainty in spectra when fitting peak models to data is reflected in the figure-of-merit and residual plots achieved by optimization.

While 33 separate spectra measured with 200 ms dwell-time might seem like a good solution to the problem of tracing the evolution in data due to systematic changes, this is not the full story. A spectrum acquired using one scan with 6.6 s dwell-time might induce different types of systematic variations in spectral intensities from a spectrum acquired using 33 scans acquired at 200ms dwell-time. Nonetheless, the experiments as described are sufficient to establish that data measured using both methods yield data for which a peak model appears to fit low signal-to-noise data with fitting statistics consistent with pulse counted data, while high signal-to-noise data exhibits suboptimal fitting statistics.

Goodness-of-Fit

Fitting a peak model to data is performed by nonlinear optimization which makes use of a figure-of-merit to identify the best fit curve formed by summing components in the peak model. The objective for optimization is to select components to minimize the figure-of-merit, but in the absence of suitable heuristics in the form of line shapes and constraints to component parameters, a figure-of-merit may and often does return fits to data that fail the test of comparison to physical outputs from the peak model. Accepting a peak model for which the fit to data does not meet the expectation of simply eliminating noise is often necessary. However, a peak model that does not fit adequately data is possibly a poor model for physical processes. So, there must be some compromise between, on the one hand, a fit capable of high-quality data reproduction resulting in a peak model for which components emerge from optimization with FWHM that are too narrow, for example, and on the other hand, accepting physically meaningful components that do not fit the data well enough to rely on the outcomes from optimization. The happy median is a fit of a peak model to data that yields, using line shapes and constraints to optimization parameters, less than optimum fitting statistics (where a suboptimal figure-of-merit can be explained through understanding sources for uncertainty in the measurement process) that also creates outputs which aid an understanding of the material. Our sense for goodness-of-fit is therefore somewhat subjective, but understandably, must rely on fitting statistics such as the figure-of-merit used in optimization coupled with visual uniformity/randomness observed in the residual plot following optimization. However, in the case of Figure 5c, the residual plot is not so random and the residual STD is not unity, therefore these fitting statistics need an explanation which follows.

Fitting statistics are now considered for Nylon data making use of N 1s spectra rather than C 1s for the following reason. A peak model such as that shown for C 1s in Figure 5c has intrinsic uncertainty. Owing to the need for four components in the peak model of unknown shape combined with the highly correlated signal from C-C-C, C-C=O and C-N chemistry, an analysis based on C 1s data from Nylon might cloud an understanding of the response of fitting statistics to optimization. Hence, to observe the consequence of fitting statistics of extending acquisition time in particular, the simple case of N 1s signal from Nylon is easier to interpret than the C 1s spectra of Nylon.

N 1s photoemission from Nylon should be a consequence of one chemical state for nitrogen. Therefore, a trivial peak model consisting of a single component representing N 1s photoemission and a background curve represented by a linear approximation is sufficient to model N 1s data from Nylon. A sequence of 33 separate spectra measured using a dwell time of 200ms provides the necessary data to trace the influence of accumulating N 1s with incrementally increasing dwell time per data bin in a spectrum. Figure 8 shows the fit of one component with asymmetric line shape LA(1,1.09,828) applied to 33 spectra formed from the original 33 N 1s spectra by summing spectra to create spectra with increments of 200 ms in dwell-time per data bin. Asymmetry is introduced via the generalized Voigt line shape Equation (8) that allows a single component to fit data (see V7 in supplementary material for the discussion on constructing line shapes) in Figure 8a with fitting statistics close to those expected for pulse counted data.

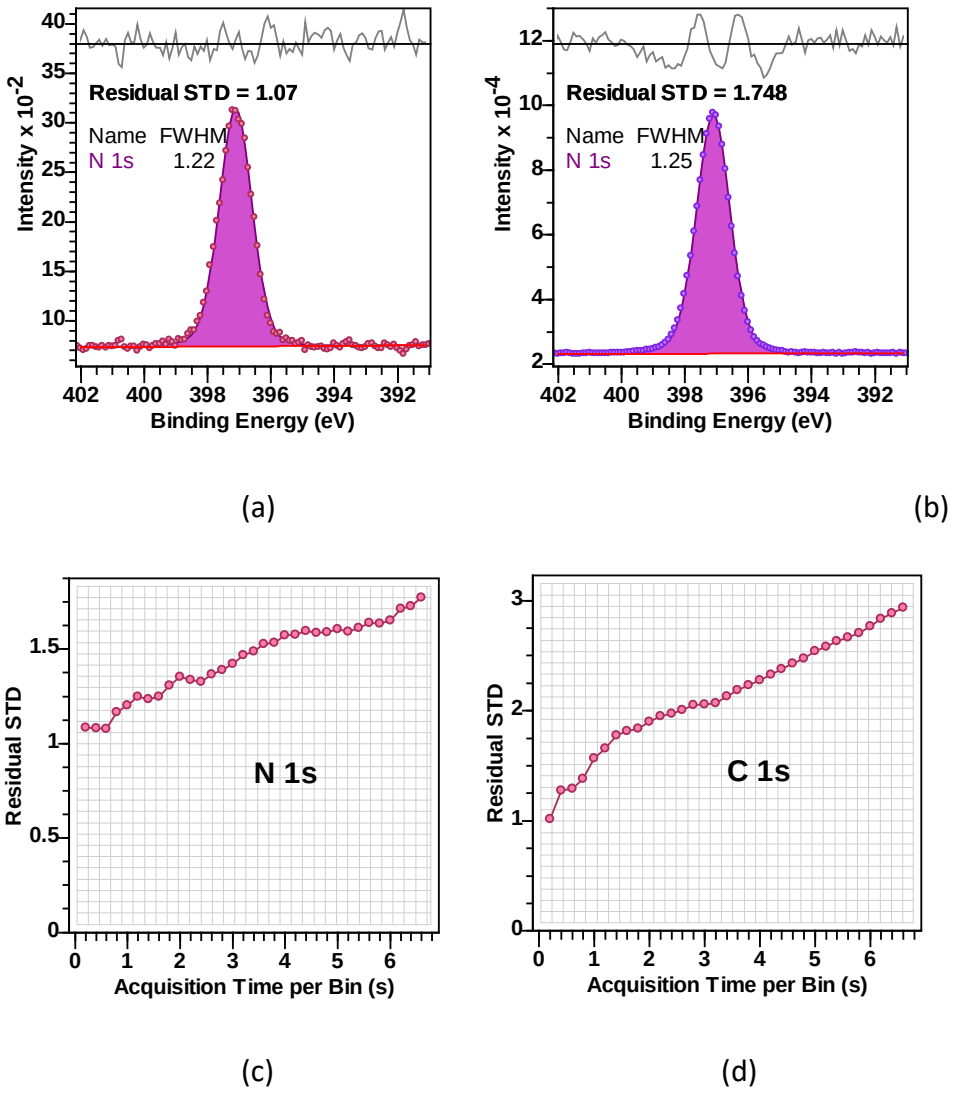

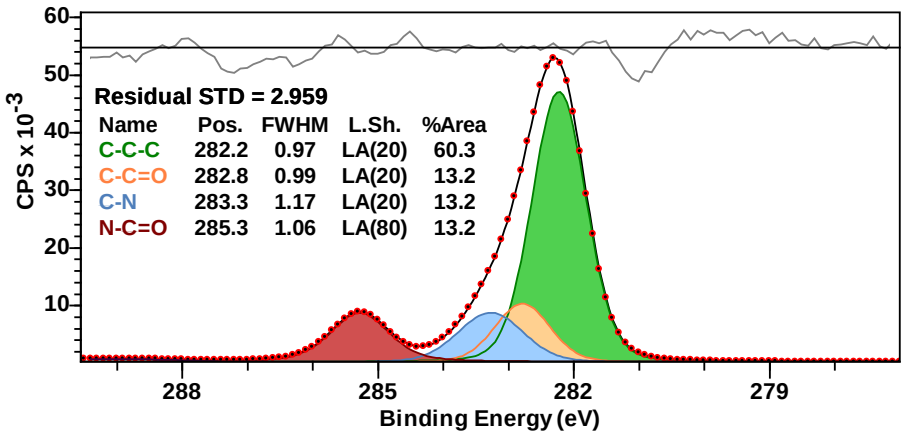

(e)

Figure 8. (a) Fit of a single component peak model to N 1s spectrum acquired using acquisition time per data bin equal to 200 ms. (b) The fit of a single component peak model to N 1s spectrum acquired using acquisition time per data bin equal to 6.6 s. (c) Profile of changes to the residual STD for fits equivalent to those shown in (a) and (b) applied to spectra with incrementally (200 ms per increment) increasing acquisition time per data bin. (d) Profile of changes to the residual STD for fits equivalent to the fit of the four-component peak model in Figure 5c applied to C 1s spectra with incrementally longer acquisition times. These C 1s spectra are similarly constructed to N 1s spectra from which the profile (c) is formed, by progressively summing 33 C 1s spectra each measured with acquisition time per data bin equal to 200 ms. (e) C 1s spectrum constructed by summation of 33 individually acquire C 1s spectra fitted with the peak model used in Figure 5c. Note the similarity in the residual shape between Figure 5c and Figure 8e.

Figure 8a is the first spectrum in the sequence of spectra acquired with dwell-time per data bin equal to 200ms. The spectrum in Figure 8b is the fit of the peak model in Figure 8a to the spectrum obtained by summing all 33 individually acquired spectra. These two spectra and fits of the same peak model to data are examples of spectra used to monitor changes to the residual STD when the same peak model is fitted to data with increasing dwell time per data bin (Figure 8c). Note how the residual STD for data acquired with short acquisition times in Figure 8a appears to suggest superior data reproduction than the residual and residual STD in Figure 8b (where the acquisition time is 33 times longer than for the data in Figure 8a). An explanation for these differences in fitting statistics is that, for the lower signal-to-noise data in Figure 8a, systematic differences between the peak model and data are less important to fitting statistics than the better signal-to-noise data in Figure 8b. Accumulating counts for N 1s 33 times longer than the data in Figure 8a allows systematic shapes to accumulate and dominate random noise, hence the residual plot in Figure 8b exhibits a shape structure which is not immediately obvious in the residual plot in Figure 8a. The trend plot of residual STD in response to increasing acquisition time per data-bin demonstrates that the shapes seen in the residual plot in Figure 8b progressively grow with each increment in acquisition time. The implication from the analysis leading to the results in Figure 8 is that fitting statistics for data collected with good signal-to-noise should not be

expected to conform to the fitting statistics expected for pulse-counted data. Similarly, low signal-to-noise data when fitted with a peak model that returns fitting statistics expected for pulse counted data should not be seen as returning a physically superior result to high signal-to-noise data for which fitting statistics appear to be inferior.

A similar analysis to that performed for N 1s shown in Figures 8a, 8b and 8c can be performed for the corresponding C 1s data measured as part of the same experiment that generated both N 1s and C 1s spectra, each with acquisition-time per data bin equal to 200ms. The results for C 1s data are comparable to that obtained from N 1s, in the sense that accumulating signal for longer periods alters the fitting statistics for the peak model in Figure 5c applied to these C 1s spectra with incrementally longer acquisition times as shown in Figure 8d. Note that the residual STD and residual plots (Figure 8e) for the constructed spectrum with acquisition time equal to the acquisition time invested when measuring the spectrum in Figure 5c are very similar. Similarity of responds of fitting-statistics between C 1s and N 1s suggests systematic errors affect both measurements. That is, there is at least circumstantial evidence C 1s photoemission peaks contain shapes similar to the shape used for N 1s, suggesting asymmetry used for N 1s may also be required for C 1s, but the flexibility offered by fitting of four C 1s components prevents a choice for line shape parameters in the same way an asymmetric line shape was determined for isolated N 1s photoemission. Hence, the desire to make use of N 1s data when attempting to observe how measurement time alters fitting statistics.

The trends for both N 1s and C 1s fitting statistics as illustrated in Figure 8 show that increasing acquisition time tends to alter the source for uncertainty in data-bins. For short acquisition times, random noise associated with pulse counted data tends to dominate uncertainty in intensity, but as acquisition times are extended, systematic errors increase and, for the examples presented in this paper, shapes induced in spectra by systematic factors dominate the source for uncertainty in data. Hence, fitting statistics for data acquired for extended periods should not be expected to follow fitting statistics expected for pulse counted data.

Constraints to Optimization Parameters

Constraints to optimization parameters are how optimization is guided towards physically acceptable solutions. The need for constraints is because optimization is purely based on mathematics and not chemistry. Nonlinear optimization applied to fitting curves to data is a general term used to describe a range of algorithms. A common theme, for these essentially different ways of determining the best fit curve to data, is that all nonlinear optimization is performed by guessing a set of parameters (used to define the curve) and then testing the quality of fit by evaluating the figure-of-merit deemed most appropriate for the data in question. Another common theme for these algorithms is that none are capable of certainty that the algorithm will deliver the true optimum set of parameters for the curve concerning the data. An important point to appreciate when working with XPS is that the minimum figure-of-merit for a given set of components in a peak model is not necessarily the best-fit-physical-curve constructed for the data. The reason the best-fit-curve differs from the best-

fit-physical-curve is that component curves are unlikely to be the exact shapes for photoemission peaks or background shapes.

When attempting to fit a peak model constructed from component curves that are not precisely the true shapes in data, the method used to prevent nonphysical outcomes from optimization involves applying constraints to optimization parameters, such as forcing two components to have equal area. Constraints to optimization parameters take two forms, namely, relational constraints which make it possible to force two components to have the same area or interval constraints. Interval constraints, as the name implies, allow parameters during optimization to take on values within a range of acceptable values. For example, a lower limit to an interval for FWHM of 0.9 eV might be considered appropriate for components defined for C 1s Nylon peak models. The objective for these constraints is to obtain by optimization a best-fit-physical-curve rather than a mathematical best-fit-curve. The example of the peak model and data in Figure 8e is an illustration of a best-fit physical curve obtained by optimization using relational constraints between component area parameters. The assumption made for the peak model in Figure 8e is that the common chemistry of a Nylon polymer is nitrogen, oxygen and one chemical state for carbon that all appear in Nylon in equal proportions. If this assumption is true, then the peak model in Figure 8e, when fitted to data, is designed to evaluate the amount of carbon bonded to carbon without influence from nitrogen and oxygen. If the assumption made is false, then the peak model must be seen as just one feasible mathematical solution for fitting data which is of limited physical meaning.

Constraints in peak models play an important role in how XPS is used. Philosophically, the primary reason peak models are constructed for XPS data is to test if a given hypothesis for the chemistry of a sample is possible. Once enough research into the chemistry of a sample has been performed to “prove” the hypothesis is true, the secondary use for a peak model is to measure chemical changes in a sample that alter the relative proportions of atoms with known chemical states. Tertiary uses for the peak model are to observe when new chemical states for atoms emerge as materials are modified or evolve. Typically, the emergence of new chemical states, manifested by a change in shapes that cannot be accounted for by alterations in intensity alone, requires a return to the primary objective for constructing a peak model, namely, to test a new hypothesis about the chemical composition of a sample by introducing additional components and applying different constraints.

Application for a Constrained Peak Model

Data from a new experiment making use of a Nylon sample is presented in Figure 9. The analysis in Figure 9a illustrates a simple use of the peak model used in Figure 5c and Figure 8e. The hypothesis for these new Nylon 6 data is that an argon-cluster ion-beam operating in a light-touch mode designed to clean a polymer surface of adventitious carbon can be used effectively for cleaning Nylon 6. These two C 1s spectra are acquired from the as-received surface and the surface the following sputtering using an argon cluster ion gun for 15 s. The peak model as designed, making use of relational constraints between area optimization parameters, returns the intensity for CH_2 chemistry that implies the as-received surface has an excess of CH_2 chemistry compared to that expected for Nylon 6. In

principle, sputtering the surface for 15 s should remove excess carbon. In practice, sputtering the surface for 15 s results in spectra for which the peak model does return the expected ratio of 1:1:1:3 for the chemical state of carbon in Nylon-6, which would appear to be a positive outcome for sputtering and the peak model.

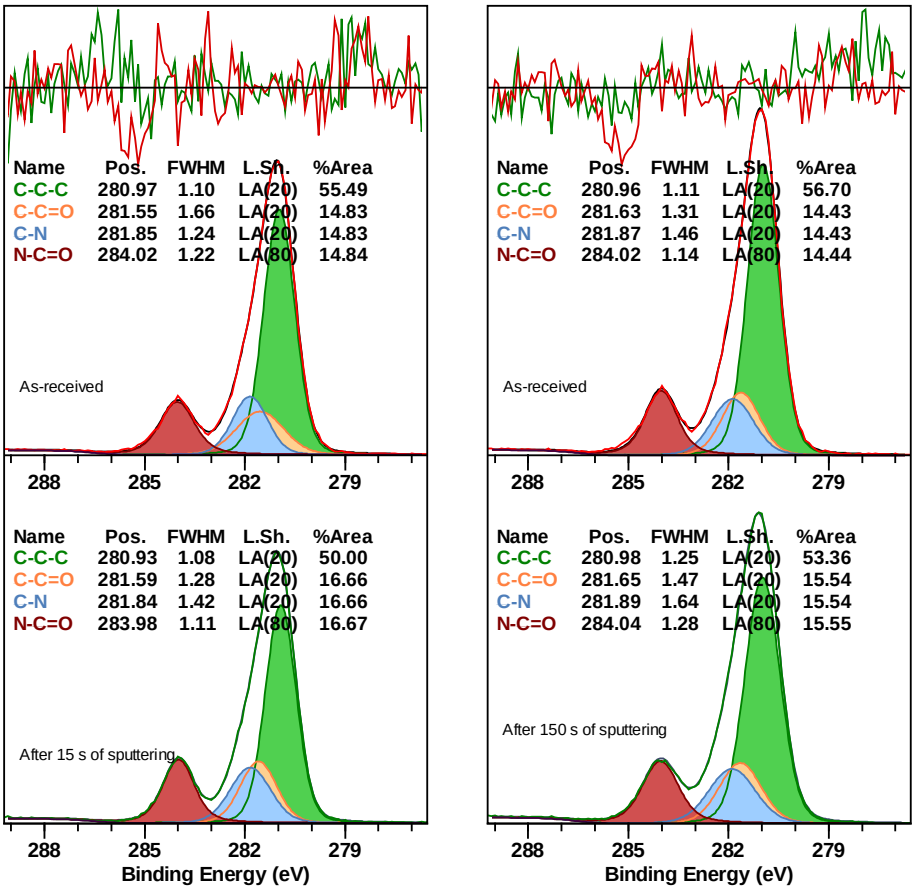

(a) (b)

Figure 9. C 1s spectra were acquired from a sample labelled as Nylon 6 which is cleaned by using an argon cluster source ion gun. Two different peak models are applied to the spectrum acquired from the as-received surface. (a) The peak model used to fit data in Figure 5c and Figure 8e was applied to two C 1s spectra measured from Nylon 6. The peak model used in (a) makes use of relational constraints for the area of the three smaller components only. (b) The peak model was obtained by fitting the peak model as defined for (a) after fitting to the spectrum labelled “After 15 s sputtering” with further constraints applied to all components for FWHM and energy. The resulting peak model is such that all components' FWHM are fixed in relative width to the FWHM of one component and the energy offset between all components is fixed relative to one energy. FWHM and energy optimization parameters, constrained by these relationships, are allowed to adjust within interval constraints which limit the parameters to ranges of values. The limits for these interval constraints do not influence the final fits as shown. The spectrum labelled “After 150 s sputtering” is acquired from the final state of the Nylon surface following 150 seconds of sputtering.

The experiment performed also attempted to find evidence of damage to the Nylon caused by sputtering through repeating sputter cycles and recording spectra following each sputter cycle. If judged purely by fitting statistics, applying the peak model in Figure 8e to these additional sputter cycles returned similar results to that obtained after the first sputter cycle. However, after inspecting the outcomes for the peak model fitted to these spectra, components show instability in FWHM and energy for components. Instability in FWHM and energy suggests constraints used to fit data in Figure 5c and Figure 8e are insufficient when applied to data with signal-to-noise characteristics as measured from sputtered Nylon. Since a different instrument was used to acquire data in Figure 9 from that used for data in Figure 8, shapes within data from the sputter experiment in Figure 9 may differ from spectral shapes in Figure 8. Hence, the analysis of the data in Figure 9 raises some discussion points as follows. Figure 9a illustrates that, despite optimization achieving a fit to data of comparable quality (visual inspection of residual traces in Figure 9a) the peak model as applied does not perform well for the as-received spectra in the sense that FWHM for C-C=O is inconsistent between as-received and sputtered Nylon in Figure 9a. Specifically, the component assigned to C-C=O changes in width (as-received FWHM 1.66eV compared to sputtered surface FWHM 1.28eV). Changes in FWHM of this nature for data measured from the same sample and instrument are difficult to justify for identical chemical states in carbon. Such changes in FWHM are possible between spectra measured using different instruments and operating modes. Hence, the level of concern raised by differences in FWHM between Figure 9b and Figure 5c is not so high as when the only difference between the two spectra is 15s sputtering with an ion gun. The general shape for the peak model between Figure 5c, Figure 8e and Figure 9a is observed in the as-received peak model. If it is proposed that the sample and peak model corresponding to the spectrum labelled “After 15 s sputtering” is most representative of Nylon 6 measured (under identical operating conditions used to acquire all spectra during the sputter experiment), then applying the peak model as stated with additional relational-constraints to force a single fitting parameter for all FWHM and a single fitting parameter for energy applied through fixed offsets between components, the new peak model alters the outcome for component areas as shown in Figure 9b. Assuming the hypothesis is correct, Figure 9b suggests that excess CH_2 chemistry is also a feature of the as-received Nylon 6 sample. The suggestion from the fits, with the additionally constrained peak model to data in Figure 9b, is that area constraints alone used in Figure 9a are insufficient to properly account for the highly correlated signal emitted from atoms with chemistry C-C-C, C-C=O and C-N. While better stability in FWHM and energy is achieved for the peak model in Figure 9b, an assumption that relational constraints imposed for FWM and energy used in Figure 9b are physically meaningful is somewhat weak, in the sense that, relying on FWHM and energy offsets determined for the highly correlated signal is in itself questionable. Nevertheless, these results shown in Figure 9 do imply Nylon 6 in an as-received state can be expected to have an excess of CH_2 chemistry. A result which is consisted of the analysis of Nylon in Figure 5c and Figure 8e.

Consequences of Constraining Optimization Parameters

The role played by constraints forcing relationships between optimization parameters has an effect on results obtained by fitting peak models to data and should not be underestimated. All peak models presented thus far assume the understanding of Nylon chemistry detailed in Figure 3b manifests directly in relative intensities for photoemission from the different chemical states. However, quantification based on survey data shown in Figure 4 suggests oxygen atoms contribute less to the XPS signal than nitrogen and carbon compared to the theoretical 1:1:6 ratio for Nylon 6 or Nylon 6,6. However, quantification results from XPS should be taken as a guide rather than an absolute statement of composition. For example, if Nylon 6 is beneath a layer or even islands of adventitious carbon, then the intensity response to the energy of lower energy electrons, such as O 1s compared to higher energy C 1s photoemission, can account for O 1s appearing less intense than C 1s signal. It is also possible the basic use of Scofield cross-sections combined with escape depth correction and assumptions about instrumental transmission response could similarly place doubt on the assertion that oxygen is less prevalent than expected for Nylon. Other arguments might be made, along the lines of that XPS induced changes to sample chemistry (not true for Nylon) or orientations for polymer backbone chemistry concerning the surface (allowing effects related to surface sensitivity) to alter photoemission intensities from those expected for a material. Therefore, any assumptions leading to constraints to optimization parameters should be compared to other plausible assumptions implemented as different relational constraints between components. The results for peak models in Figure 10 illustrate how changes to parameter constraints alter outcomes for the same data. These two fits in Figure 10 demonstrate the importance of publishing full details of how a peak model is constructed.

Beamson and Briggs, XPS of Polymer Database[5] include examples of peak models for both Nylon 6 and Nylon 6,6. For both materials, the component in the Beamson and Briggs peak models representing C 1s photoemission from the carbon of the form N-C=O is computed with an area less than C-N and C-C=O. To illustrate how results of this nature can occur, two different peak models are compared in Figure 10. These two peak models differ only in the relational constraints for the area between components. If it is assumed, as shown in Figure 10a, the area for N-C=O is allowed to be different in the area from C-N and C-C=O, but the correlated signal indicated in Figure 3a for C-N, C-C=O and C-C-C are constrained in the ratio 1:1:3, then the results of fitting this peak model to data in Figure 10a indicates N-C=O intensity is deficient compared to other carbon chemistry. The table displayed in Figure 10a presents the results of fitting the peak model to data and also includes information regarding the relational constraints applied to the component area. Each component in the peak model is listed and identified by a letter. Relational constraints for the component area are defined by these letters and a multiplicative scale factor. The table for the peak model in Figure 10a indicates the components labelled B and C are forced during optimization to maintain the area of the component labelled A multiplied by a third. Constraints of this form would be appropriate given a sample with the exact stoichiometry of Nylon 6 and all C 1s signal from any of these chemical states are measured without bias.

The peak model in Figure 10b displays a table of constraints that provides a solution that ensures N-C=O is in the same proportions as C-N, C-C=O. The outcome in terms of percentage area when these two peak models in Figure 10 are optimized concerning data is different. It is therefore clear assumptions embodied in constraints alter the interpretation of carbon chemistry. For these reasons, to permit reproducibility of published results, peak models and fits of peak models to data should include the methods used to constrain component parameters that achieve the outcomes reported. *The corollary to this statement is line shapes, which act as a constraint when fitting a peak model to data, should be reported as well as parameter constraints used.*

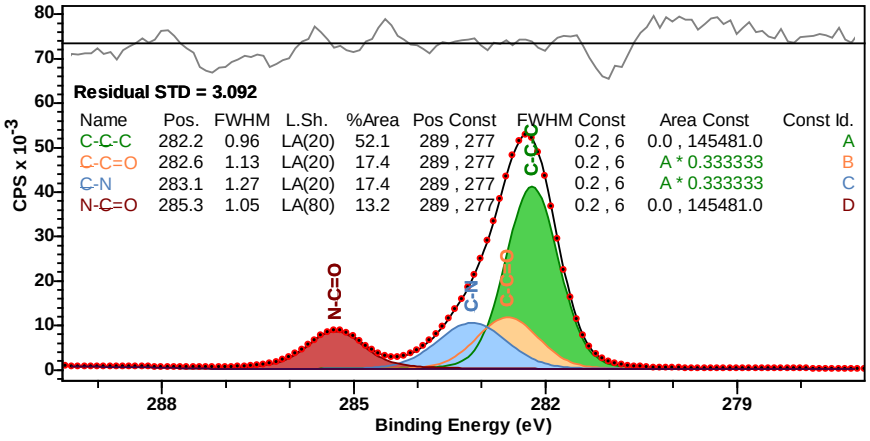

(a)

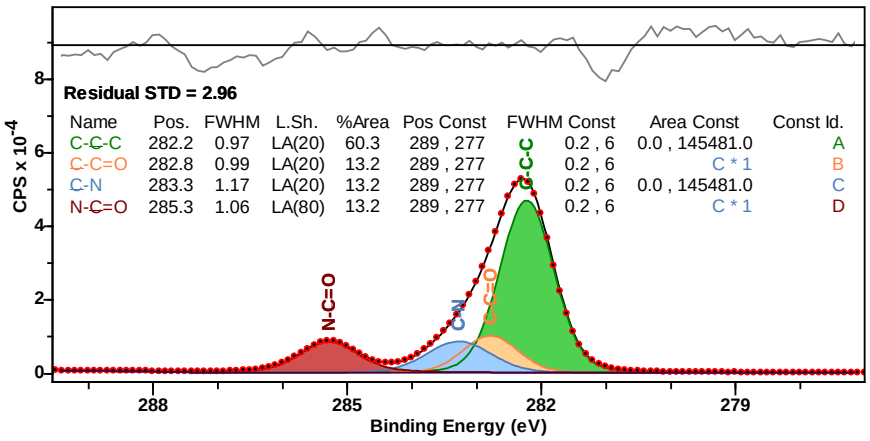

(b)

Figure 10. Two peak models for Nylon constructed with identical numbers of components, making use of identical line shapes, fitted to the same spectrum. (a) The peak model constructed assuming C-N, C-C=O and C-C-C component areas are in the ratio 1:1:3. (b) The peak model constructed assuming C-N, C-C=O and N-C=O component areas are in the ratio 1:1:1.

Conclusions

Nylon XPS spectra have been used to examine aspects of fitting bell-shaped curves to XPS data. In the course of doing so, the importance of optimization parameter constraints to a successful chemical state analysis of XPS data is demonstrated. Examples involving different peak models defined by different parameter constraints applied to C 1s spectra measured from Nylon are used to show it is possible to create different outcomes for the same set of components in a peak model. Different outcomes for the same number and shape of components in a peak model fitted to the same spectra are used to make the case for publishing both line shapes and relationships between components that influence scientific conclusions gleaned from fitting peak models to XPS data.

Peak models developed for Nylon C 1s spectra are further used to show that fitting statistics used to infer quality for a goodness-of-fit, despite being carefully constructed to reflect chemistry, do not achieve the quality of fit expected for pulse-counted data. Residual STD figure-of-merit and uniformity for residual plots do not conform to what is expected for pulse counted data, unless sufficiently short dwell-time per data-bin is used to acquire data. At each stage in the construction of peak models, aspects of XPS are presented to explain, for data acquired over time intervals that allow systematic deformations in data to accumulate, why it is unreasonable to expect mathematically defined line shapes to fully describe photoemission as measured. The role of fitting statistics with fitting curves to data has been discussed. In particular, measures for goodness-of-fit are shown to be dependent on the way data are acquired and the expected residual standard deviation of unity for pulse counted data is unrealistic for data acquired over extended periods. The conclusion is that peak models designed with imperfect line shapes, compensated for by appropriate optimization parameter constraints to provide an adequate description for chemical properties, do not necessarily yield well-formed residual plots nor is it required to fit data with a residual standard deviation of unity.

Acknowledgments

This work by J.B. was supported as part of UNCAGE-ME, an Energy Frontier Research Center funded by the U.S. Department of Energy, Office of Science, Basic Energy Sciences under Award No. DE-SC0012577. The CNRS is acknowledged for financial support to the Thematic Workshop (N° 1317144) held at the Station Biologique, Roscoff, France.

Author contributions

Neal Fairley: Investigation (supporting); Methodology (lead); Writing – review and editing (equal). Vincent Fernandez: Investigation (equal); Writing – review and editing (equal). Pascal Bargiela: Investigation (equal); Writing – review and editing (equal). Adam Roberts: Investigation (equal); Jonas Baltrusaitis: Methodology (supporting); Supervision (lead); Writing – review and editing (equal).

Supporting information

Tutorials on the spectral manipulation of the data described in this work using CasaXPS [16] software is presented in the form of the tutorial videos as follows.

V1 https://www.youtube.com/watch?v=jmspJZJLQYQ

[V2] https://www.youtube.com/watch?v=0j1D7I_lunk

[V3] https://www.youtube.com/watch?v=7OmXWkjteT4

[V4] https://www.youtube.com/watch?v=coIqqurUEfk

[V5] https://www.youtube.com/watch?v=VWlaPmC1N3A

[V6] https://www.youtube.com/watch?v=4x8sMDb_MxY

[V7] https://www.youtube.com/watch?v=rIo5o0JPaTI

References

[1] G.H. Major, N. Fairley, P.M.A. Sherwood, M.R. Linford, J. Terry, V. Fernandez, and K. Artyushkova, J. Vac. Sci. Technol. A **38**, 061203 (2020).

[2] B. Moeini, M.R. Linford, N. Fairley, A. Barlow, P. Cumpson, D. Morgan, V. Fernandez, and J. Baltrusaitis, Surf. Interface Anal. (2021).

[3] K. Harrison and L.B. Hazell, Surf. Interface Anal. **18**, 368 (1992).

[4] P.J. Cumpson and M.P. Seah, Surf. Interface Anal. **18**, 345 (1992).

[5] G. Beamson and D. Briggs, *High Resolution XPS of Organic Polymers: The Scienta ESCA300 Database* (Wiley; 1st edition, 1992).

[6] G.H. Major, V. Fernandez, N. Fairley, and M.R. Linford, Surf. Interface Anal. **54**, 262 (2022).

[7] M.C. Biesinger, Appl. Surf. Sci. **597**, 153681 (2022).

[8] Ian W. Drummond, in *Surf. Anal. by Auger X-Ray Photoelectron Spectrosc.*, edited by D. Briggs and J.T. Grant (IMPublications, Chichester, UK and SurfaceSpectra, Manchester, UK, 2003), p. 899.

[9] A.M. Mood, F.A. Graybill, and D.C. Boes, *Introduction to the Theory of Statistics*, 3rd ed. (McGraw Hill, 1973).

[10] M.C. Biesinger, B.P. Payne, A.P. Grosvenor, L.W.M. Lau, A.R. Gerson, and R.S.C. Smart, Appl. Surf. Sci. **257**, 2717 (2011).

[11] B.M. Garland, N. Fairley, N.C. Strandwitz, R. Thorpe, P. Bargiela, and J. Baltrusaitis, Appl. Surf. Sci. **598**, 153827 (2022).

[12] D.A. Shirley, Phys. Rev. B **5**, 4709 (1972).

[13] S. Tougaard, Surf. Interface Anal. **11**, 453 (1988).

[14] A.G. Shard, J. Vac. Sci. Technol. A **38**, 041201 (2020).

[15] D. Briggs and G. Beamson, Anal. Chem. **64**, 1729 (1992).

[16] N. Fairley, V. Fernandez, M. Richard-Plouet, C. Guillot-Deudon, J. Walton, E. Smith, D. Flahaut, M. Greiner, M. Biesinger, S. Tougaard, D. Morgan, and J. Baltrusaitis, Appl. Surf. Sci. Adv. **5**, 100112 (2021).